Müller and Regenspurg *Geotherm Energy (2017) 5:25*
DOI 10.1186/s40517-017-0080-1

Geothermal Energy

RESEARCH Open Access

The element-release mechanisms of two pyrite-bearing siliciclastic rocks from the North German Basin at temperatures up to 90 °C under oxic and anoxic conditions

Daniel Richard Müller* and Simona Regenspurg

*Correspondence: daniel.mueller@gfz-potsdam.de
Section 6.2: Geothermal Energy Systems, GFZ German Research Centre for Geosciences, Telegrafenberg, 14473 Potsdam, Germany

Abstract

Leaching tests with synthetic brines (25 g/L NaCl) between 25 °C and 90 °C were performed under oxic and anoxic conditions over 7 days on two pyrite-bearing siliciclastic rocks from the Lower Jurassic Hettangian and Sinemurian stages in the North German Basin. The release mechanisms of the mobile elements Al, As, Ba, Ca, Cu, Fe, Mn, Ni, Si, and Pb were studied and explained by means of numerical simulations of the leaching tests. The study was performed in the context of aquifer thermal energy storage (ATES) to improve the understanding of water–rock interactions during heat storage. Results showed that release patterns of Ba, Ca, Cu, Fe, Ni, and Pb were predominantly controlled by the dissolution of pyrite under oxic conditions and iron hydroxides under anoxic conditions. The mobilizations of Al and Mn could be explained by a combination of desorption and the dissolution of hydroxides. Si was mainly released from amorphous silica. The mobilization of Ca was governed by pH-sensitive desorption and calcite dissolution in one of the samples. Arsenic was immobile in both studied rocks. In general, elemental release was augmented by the presence of oxygen and the subsequent dissolution of pyrite and reduction of pH, which should therefore be avoided in ATES systems.

Keywords: Sandstone, Pyrite oxidation, Aquifer thermal energy storage, Rock reactivity, PhreeqC, Numerical simulation, Leaching test

Background

Over the last few decades, shallow geothermal systems (< 400 m depth) have been increasingly utilized as renewable energy sources and storage systems for heating and cooling for domestic and public use (e.g., Bayer et al. 2012; Blum et al. 2010; Fridleifsson et al. 2009; Lund et al. 2011). Aquifer thermal energy storage (ATES) facilities directly use aquifers for seasonal storage of thermal energy. In summer, groundwater is produced from the storage aquifer, heated up with excess energy, and reinjected into the aquifer. In winter, the stored thermal energy is withdrawn from the water by reversing the process. That way, storage of cooling energy is possible as well (Hähnlein et al. 2010; Kranz and Bartels 2009; Kranz and Frick 2013). The reliability and efficiency of ATES systems can be affected by fluid mixing and changes in temperature and pressure in the storage

Springer Open

© The Author(s) 2017. This article is distributed under the terms of the Creative Commons Attribution 4.0 International License (http://creativecommons.org/licenses/by/4.0/), which permits unrestricted use, distribution, and reproduction in any medium, provided you give appropriate credit to the original author(s) and the source, provide a link to the Creative Commons license, and indicate if changes were made.

aquifer during operation, which induces chemical reactions such as desorption and mineral dissolution or precipitation. Subsequently, physicochemical water properties like pH or redox potential may change, and mobilized elements may precipitate and clog the aquifer, block pipes, or form coatings that reduce the efficiency of the heat exchanger. If the ATES system is built in an aquifer that serves as drinking water supply as well, the release of toxic elements such as heavy metals need to be avoided (Bonte et al. 2013a, Possemiers et al. 2014). Altered water properties may promote corrosion or induce subsequent fluid–rock interactions (Allen et al. 1984; Frick et al. 2011; Palmer et al. 1992). To avoid aquifer damage by clogging, corrosion or contamination, legal regulations in several countries limit the groundwater temperature change to a maximum of 3 to 11 K, as the effects of large temperature variations on dissolution, desorption and microbial communities are still poorly understood (Hähnlein et al. 2010). If deeper aquifers are used for ATES systems, either to avoid potential contamination of freshwater aquifers or to improve the heat recovery factor (Kranz and Bartels 2009), the impact of increased salinity needs to be considered as well. Several research projects investigated the feasibility of heat storage systems designed for up to 90 °C. Field monitoring campaigns over several years (e.g., Huenges 2011; Wolfgramm and Seibt 2006) were complemented by experiments in controlled environments, investigating both abiotic and microbially catalyzed hydrogeochemical reactions. Arning et al. (2006) investigated the reactivity of siliciclastic shallow aquifer sediments from the North German Basin at up to 50 °C, and observed increased solubility of silicates, particularly potassium feldspar. Jesußek et al. (2013) reported temperature-dependent redox shifts toward reducing conditions in column experiments with siliciclastic sediments from the North German Basin between 10 and 70 °C. Distinct cation release was only observed at 70 °C. Bonte et al. (2013a) performed column experiments with anoxic unconsolidated aquifer sands between 5 and 60 °C and reported significant increases in element solute concentrations at 60 °C, while the sediment remained only slightly reactive at lower temperatures. Consistent element-release patterns were only partially observed, e.g., for silicium and potassium. Adaptations of the microbial communities to temperature changes in both composition and quantity were found in field-monitoring campaigns (Vetter et al. 2012; Würdemann et al. 2014) and in the laboratory (Bonte et al. 2013b).

While these studies qualitatively interpret the fluid–rock interactions responsible for the observed changes in physicochemical water properties and ion release, the differentiation and quantification of the individual release mechanisms, such as mineral dissolution and desorption, remain difficult. Since knowledge of the release mechanisms is necessary to understand and predict reactions of the aquifer chemistry to changes in environmental parameters induced by ATES system operation, such as temperature or solute oxygen, this study utilizes extraction experiments and numerical simulations to quantify the reactivity of aquifer rocks under these conditions. It focuses on siliciclastic rocks at temperatures between 25 and 90 °C and under shifting redox conditions due to the introduction of dissolved oxygen into normally oxygen-depleted aquifers. In this context, pyrite (FeS_2) is the most important mineral, since it is ubiquitous and occurs in many sedimentary rocks used for ATES storage. It has a high sensitivity to changes under redox conditions and the potential to acidify the surrounding groundwater upon dissolution (Nordstrom 1982). The short-term reactivities of two siliciclastic rocks with

synthetic, saline groundwater under controlled laboratory conditions that mimic conditions in a thermal aquifer storage system were investigated to study their dependence on temperature. Experimental results were complemented by numerical simulations to help explain and quantify the observed release mechanisms.

Methods

Materials

Weakly consolidated rock material was sampled from two Lower Jurassic horizons in the North German Basin, which are used for aquifer thermal energy storage. The samples were collected in the ATES well "Am Reichstag 2/98," situated in the city of Berlin (Germany). Sample I was taken from the Hettangian aquifer in a depth of 310 m ("Hettangian sandstone"). It is a fine sandstone containing 95% quartz and 1–2% potassium feldspar, muscovite, and kaolinite each with minor and trace phases (< 1%) comprising rutile (TiO_2), ilmenite ($FeTiO_3$), pyrite (FeS_2), iron hydroxides, and 0.1% organic matter (Müller et al. 2017). Sample II was taken from the hanging Sinemurian aquiclude at a depth of 297 m ("Sinemurian siltstone"). It is a fine siltstone comprising 39% quartz, 37% clay minerals, 12% mica, and 8% potassium feldspar. Minor and trace phases (ca. 4%) contain the same minerals as sample I and 1.2% organic matter (ibid.). The mobilities and phase associations of several elements were determined by sequential extraction (ibid.), differentiating between exchangeable, acid-soluble (carbonates), reducible (oxides and hydroxides), and oxidizable (organic matter and sulfides) phases. The results of the extraction of 1 g rock with 30 mL of solvent are displayed in Fig. 1.

The two rock samples were ground in a mortar to obtain a homogeneous powder with the original grains kept intact. After grinding, the material was washed carefully for 1 h with ultrapure water purged with nitrogen and dried overnight at 70 °C.

The synthetic saline groundwater utilized in the extraction experiments was prepared from ultrapure water and 25 g/L analytic grade sodium chloride (NaCl), which corresponds to the salinity of the Hettangian aquifer. In addition to Na^+ and Cl^-, the natural groundwater contains 0.86 g/L of other solute species, mainly Ca^{2+} (0.29 g/L), SO_4^{2-} (0.25 g/L), and Mg^{2+} (0.24 g/L) (Huenges 2011).

Leaching experiments

Leaching tests were performed at room temperature (25 °C), 50, 70, and 90 °C, over 1, 2, 4, and 7 days under oxic and anoxic conditions. The experiments were carried out in triplicate with 1 g of rock material and 30 ml of synthetic groundwater. Manual shaking was applied every 24 h. The redox potential of the synthetic groundwater before leaching was 192 mV under oxic conditions and 105 mV after purging with nitrogen under anoxic conditions, as determined using a WTW SenTix 940 electrode connected to a WTW Multi 3420 multimeter.

For tests under oxic conditions, the rock material and synthetic groundwater were filled into 60-ml PP bottles, which were placed in a lab oven and heated up to the desired temperature. After leaching, rock material and eluate were separated by filtration using filter papers. The pH of the eluates was determined using WTW Sentix 81 electrodes connected to a WTW Multi 340i multimeter before acidizing the eluates to pH < 2 using 65% HNO_3.

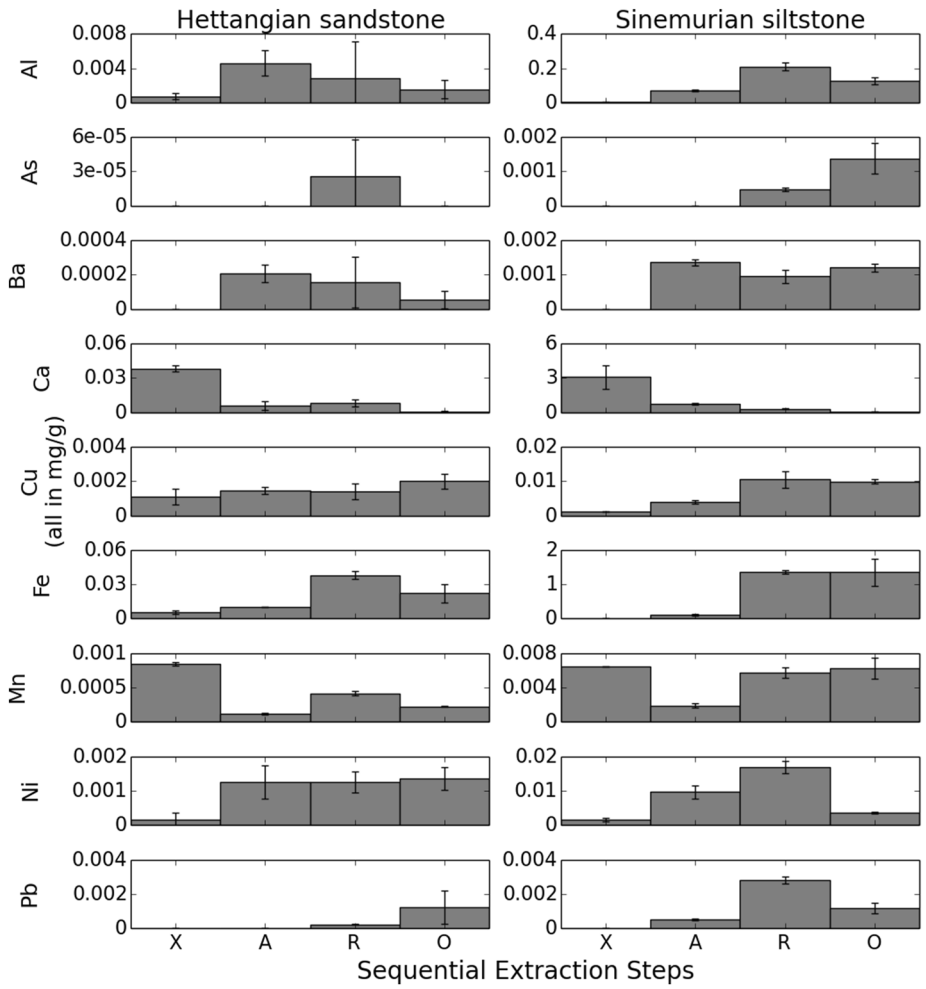

Fig. 1 Mass fractions (mg/g sediment) and phase associations of mobile elements in the sampled rocks, as determined by sequential extraction with 1 g of rock and 30 mL of solvent. The phases are *X*, exchangeable; *A*, acid-soluble; *R*, reducible; *O* oxidizable Data taken from Müller et al. (2017)

To maintain anoxic conditions, all experiments were performed in an Ar (5% H_2)-purged glovebox. The oxygen concentration in the gas phase was maintained at less than 10 ppm throughout the experiment. The synthetic groundwater was purged with nitrogen to < 0.1 mgl solute oxygen, as determined using a WTW FDO 925 probe with a WTW Oxi 3310 acquisition unit. Inside the glovebox, ground rock samples and synthetic groundwater were filled into 50-ml centrifuge tubes, which were placed on heating plates equipped with stainless steel fittings to ensure a stable temperature distribution. After extraction, rock material and eluates were separated inside the glovebox by filtration using filter papers, and the eluates were decanted into 60-ml PP bottles, which were sealed against the atmosphere with Parafilm. The pH of the eluates was determined outside the glovebox by means of WTW Sentix 41 and 81 electrodes connected to a WTW Multi340i multimeter. Afterward, the eluates were acidized to pH < 2 with 65% HNO_3.

The solute concentrations of aluminum (Al), arsenic (As), barium (Ba), calcium (Ca), copper (Cu), iron (Fe), manganese (Mn), nickel (Ni), lead (Pb), and silicium (Si) were

determined by inductively coupled plasma optical emission spectrometry (ICP-OES, Thermo Scientific iCAP 6300 Duo).

For the results of the leaching experiments, correlation matrices were calculated utilizing Pearson's method to help identify possible relationships between the extracted concentrations, pH, time, and temperature. Calculations were performed using the library "Pandas" (McKinney 2010) for the high-level programming language, Python. The complete matrices are provided as Additional file 1. The correlation between the individual parameters was categorized into three groups: "strong correlation" for correlation coefficients (r) between 0.68 and 1; "modest" or "moderate correlation" for r between 0.36 and 0.67; and no correlation for $r \leq 0.35$ (Taylor 1990).

Numerical simulation

Numerical simulations were performed using the software PhreeqC, version 3.3.7 (Parkhurst and Appelo 2013), for the release mechanisms of the main mineral-forming elements Al, Ca, Fe, Mn, and Si. For statistical analyses, the IPhreeqC module was accessed by Python scripts by means of the PhreeqPy interface (Müller 2013). Statistical analyses were performed by means of the Python libraries "Pandas" (McKinney 2010), "NumPy," and "SciPy" (van der Walt et al. 2011). The workflow comprised the following steps:

1. Defining the brine composition and the initial mineral content.
2. Compiling relevant thermodynamic and kinetic data and calibrating them with the results of the leaching experiments.
3. Conducting a sensitivity analysis to identify the influence of different release mechanisms to the final solute element concentrations.
4. Calculating the goodness-of-fit of the simulation to the experimental results and repeating steps 1 to 3 as required.

In the first step, the initial synthetic groundwater was modeled as a 25 g/l (0.44 M) NaCl solution with pH 7. The initial pe values obtained from measurements were 3.3 for the oxic brine, and 1.8 for the anoxic brine. The mineral composition data for both rocks were taken from Müller et al. (2017). Minerals considered were quartz, amorphous silica, potassium feldspar, kaolinite, muscovite, calcite, pyrite, amorphous ferrihydrite, amorphous aluminum hydroxide, and manganese oxohydroxide. Since the mass fraction of amorphous aluminum hydroxide had not been calculated before, the amount was estimated from the Al released during the acid-dissolution step of the sequential extraction (Müller et al. 2017), based on the assumption that the hydroxides would completely dissolve at pH 3.7 (Marion et al. 1976). The mass fraction of amorphous silica was unknown as well. The fast initial release of Si observed in the leaching tests (Figs. 2, 3, 4, 5) was attributed to amorphous silica dissolution, after calibrations found that crystalline silicate dissolution was too slow to explain it. This effect is common and has been described in other studies (e.g., Rimstidt and Barnes 1980). The mass fraction of amorphous silica was subsequently fitted to the experimental results using least squares regression. The final input mineral composition is shown in Table 1.

Table 1 Minerals and exchangers considered in the model

Phase	Composition	Mass fraction, %		Reactive surface, m^2/g	
		Sample I	Sample II	Sample I	Sample II
Quartz	*SiO_2*	*95*	*39*	*0.002*	*0.02*
Amorphous silica	$SiO_{2\ (amorph)}$	0.0001	0.0009	300	300
Potassium feldspar	*$KAlSi_3O_8$*	*2*	*8*	*0.0023*	*0.023*
Kaolinite	$Al_2Si_2O_5(OH)_4$	1	37	3.6	3.6
Muscovite	$KAl_3Si_3O_{10}(OH)_2$	1	12	1.2	1.2
Calcite	$CaCO_3$	*0*	0.2	*0*	0.0001
Pyrite	FeS_2	0.005	0.29	0.003	0.001
Ferrihydrite	$Fe(OH)_{3\ (amorph)}$	0.007	0.26	n.a.	n.a.
Aluminum hydroxide	$Al(OH)_{3\ (amorph)}$	0.0013	0.02	n.a.	n.a.
Manganese oxohydroxide	MnOOH	0.0007	0.0004	n.a.	n.a.
Al exchange	AlX_3	7.3×10^{-5}	2.6×10^{-4}	n.a.	n.a.
Ca exchange	CaX_2	3.8×10^{-3}	0.3	n.a.	n.a.
Mn exchange	MnX_2	8.4×10^{-5}	6.4×10^{-4}	n.a.	n.a.

Phases printed in italics were excluded after sensitivity analysis or initial simulations. Mass fractions were taken from Müller et al. (2017), except amorphous aluminum hydroxide, which was calculated from sequential extraction data (ibid.). Reactive surfaces were calculated from specific surface values collected in the RES^{3}T database

Phases printed in italics were excluded after sensitivity analysis or initial simulations

In the second step of the workflow, comprising reaction data compilation and calibration, thermodynamic data were taken primarily from the LLNL database integrated in PhreeqC. Amorphous ferrihydrite was modeled using the log K value from the SIT database, which is also included in the PhreeqC package, and the standard enthalpy of reaction (ΔH) from the LLNL database. Data for amorphous aluminum hydroxide were taken from Kittrick (1969). No ΔH values were available for amorphous aluminum hydroxide and manganese oxohydroxide, so no direct temperature dependence could be calculated for these two phases. The data for all considered reactions are compiled in Table 2.

Data for kinetic mineral dissolution were adopted from Palandri and Kharaka (2004). The formulation for the kinetic dissolution of minerals given therein is as follows:

Table 2 Dissolution reactions considered in the model

Phase	Reaction	Log K	ΔH (KJ/mol)
Amorphous silica	$SiO_{2(am)} \leftrightarrow SiO_{2(aq)}$	− 2.71	20.05
Kaolinite	$Al_2Si_2O_5(OH)_4 + 6H^+ \leftrightarrow 2Al^{3+} + 2SiO_{2(aq)} + 5H_2O$	6.81	− 151.8
Muscovite	$KAl_3Si_3O_{10}(OH)_2 + 10H^+ \leftrightarrow 3Al^{3+} + K^+ + 3SiO_{2(aq)} + 6H_2O$	13.6	− 243.2
Calcite	$CaCO_3 + H^+ \leftrightarrow Ca^{2+} + HCO_3^-$	1.85	− 25.71
Pyrite	$FeS_2 + 3.5O_2 + H_2O \leftrightarrow Fe^{2+} + 2SO_4^{2-} + 2H^+$	217.4	− 1412
	$FeS_2 + 14Fe^{3+} + 8H_2O \leftrightarrow 15Fe^{2+} + 2SO_4^{2-} + 16H^+$	98.5	− 50.69
Ferrihydrite	$Fe(OH)_3 + 3H^+ \leftrightarrow Fe^{3+} + 3H_2O$	2.54	− 84.08
Amorphous aluminum hydroxide	$Al(OH)_3 + 3H^+ \leftrightarrow Al^{3+} + 3H_2O$	9.7	–
Manganese oxo-hydroxide	$MnOOH + 3H^+ \leftrightarrow Mn^{3+} + 2H_2O$	− 0.16	–

Data taken from the LLNL database, except log K of ferrihydrite (SIT database) and amorphous aluminum hydroxide (Kittrick 1969). Values for the standard enthalpy of formation ΔH for amorphous aluminum hydroxide and manganese oxohydroxide are not available in the databases

$$\frac{\mathrm{dm}}{\mathrm{dt}} = -A_{\mathrm{surf}} \left[\begin{array}{l} k_{\mathrm{acid}}^{298.15\mathrm{k}} \mathrm{e}^{\frac{-E_{\mathrm{acid}}}{R}\left(\frac{1}{T}-\frac{1}{298.15\ \mathrm{K}}\right)} a_{\mathrm{H^+}}^{n_1} (1-\Omega^{p_1})^{q_1} \\ + k_{\mathrm{neut}}^{298.15\ \mathrm{K}} \mathrm{e}^{\frac{-E_{\mathrm{neut}}}{R}\left(\frac{1}{T}-\frac{1}{298.15\ \mathrm{K}}\right)} (1-\Omega^{p_2})^{q_2} \\ + k_{\mathrm{base}}^{298.15\ \mathrm{K}} \mathrm{e}^{\frac{-E_{\mathrm{base}}}{R}\left(\frac{1}{T}-\frac{1}{298.15\ \mathrm{K}}\right)} \mathrm{a}_{\mathrm{H^+}}^{n_3} (1-\Omega^{p_3})^{q_3} \end{array} \right] \quad (1)$$

In this formula, dm/dt is the mineral mass reduction over time (kg/s), A_{surf} is the reactive surface area (m^2), k_m 298.15 K is a theoretical rate constant at 25 °C and pH 0 for a mechanism m; E_m is the activation energy for a mechanism m (J/mol); R is the universal gas constant (J/kg/mol); T is the temperature (K); a_{H+} is the activity of H^+; Ω is the mineral saturation index; and p_i and q_i are empirical constants. With the exception of the reactive surface area, which is an individual fraction of the specific surface area that depends on sample structure and texture (Lasaga 1998), these data were compiled from the article by Palandri and Kharaka (2004) for all minerals considered in the present study. Kinetically retarded dissolution was assumed for quartz, amorphous silica, potassium feldspar, kaolinite, muscovite, calcite, and pyrite. Thermodynamic equilibria were assumed for ferrihydrite, amorphous aluminum hydroxide, and manganese oxohydroxide. To obtain the reactive surface areas, first the specific surface areas A_{spec} were determined. For quartz and potassium feldspar, A_{spec} values were calculated geometrically assuming spheric shape with $A_{\mathrm{spec}} = 3/(r \cdot \rho_m)$, where r is the average grain radius and ρ_m the grain density. The average grain radius was set to 50 µm for sample I (fine sandstone), and to 5 µm (fine siltstone) for sample II. The grain radii had been determined by scanning electron microscopy (SEM) utilizing a Carl Zeiss SMT Ultra 55 Plus machine, coupled with energy-dispersive X-ray spectroscopy (EDX) by means of a Thermo Fisher Scientific UltraDry SDD EDX detector for mineral identification. Grain density is 2650 kg/m^{-3} for quartz and 2600 kg/m^{-3} for potassium feldspar (Deer et al. 1992). The average grain sizes and grain shapes of the other solid phases contained in the rock were unknown, and therefore, the median values of the specific surface values collected from numerous literature sources in the RES^{3}T database (Brendler et al. 2003) were used as a reference. The specific surface values for each solid phase were multiplied with a factor of 3 to match the measured BET surface values of 0.5 m^2/g for sample I, and 13.2 m^2/g for sample II, as reported by Müller and Regenspurg (2014). The resulting specific surface values were within the range of literature values compiled in the RES^{3}T database. To account for the fact that only some of the grain surfaces are involved in dissolution reactions (Lasaga 1998), the reactive surfaces were estimated by reducing the specific surfaces stepwise to find the best fit to the data from the leaching tests. The specific surface was consequently reduced by one order of magnitude for all solid phases except pyrite and amorphous silica. For amorphous silica, half of the specific surface was assumed to be reactive. For pyrite, the reactive surface was fitted to the experimental data by matching the solute iron concentrations observed during dissolution under oxic conditions, assuming that reprecipitation and re-adsorption were negligible due to small solute concentrations (Sulkowski 2002). Fitting was performed with least squares regression (Table 1).

Exchange reactions were calculated for Al, Ca, and Mn assuming unspecific bulk sorption, where the exchangeable amount per rock mass was taken from the exchange step of the sequential extraction performed by Müller et al. (2017).

In the third step of the workflow, a sensitivity analysis was performed to identify the contribution of various release mechanisms to solute Al, Si, and Fe concentrations. Ca and Mn have only one mineral contributing to their respective solute concentrations, and were thus not analyzed. As input parameters, all minerals and exchangers potentially releasing the investigated solute element were considered, as well as physicochemical water parameters. The mineral mass fractions and exchangeable amounts were varied between 0 and the fitted initial values displayed in Table 1, pe was varied between 1.8 (anoxic) and 3.3 (oxic), and oxygen was varied between 0 (anoxic) and "abundant supply" (oxic). Pyrite was selected as the controlling variable for pH. Temperature and reaction time were set to constant values. For Fe, only oxic mobilization was considered. The sensitivity analysis was performed by means of the Python library "SALib" (Herman et al. 2017). For each input parameter, seven samples within their respective boundaries were drawn and analyzed utilizing the quasi-Monte Carlo-type Sobol method (Sobol 2001; Saltelli 2002; Saltelli et al. 2010). As outputs, the total-order sensitivity indexes were calculated. They measure a combination of the first-order sensitivity of an input parameter and the higher-order sensitivities which quantify synergetic effects between multiple input variables (Homma and Saltelli 1996).

In the fourth step of the workflow, the goodness-of-fit of the simulation was measured using the normalized root mean square error (NRMSE). The NRMSE was calculated for each solute element and temperature using the equation:

$$\mathrm{NRMSE} = \frac{\sqrt{\sum_{t_{\min}}^{t_{\max}} (c_\mathrm{s} - c_\mathrm{m})^2}}{\overline{C_\mathrm{m}}}, \tag{2}$$

where $t_{\min}$ and $t_{\max}$ are the first and last time steps, respectively, c_s is the simulated solute concentration, c_m is the measured solute concentration, and $\overline{C_\mathrm{m}}$ is the arithmetic mean of all measured solute concentrations.

Results

Experimental study: leaching test

In both the Hettangian sandstone and the Sinemurian siltstone, the most mobile elements were Al, Ca, Fe, and Si, followed by Mn. Only traces of Ba, Cu, Ni, and Pb were mobilized. Arsenic was generally immobile.

During the leaching of samples of the Hettangian sandstone, the pH decreased over time, with the magnitude of the decrease depending on temperature and the presence of oxygen. The lowest pH under oxic conditions was 3.7, and 5.0 under anoxic conditions (Figs. 2 and 3). The concentrations of Al, Ca, Fe, and Si released from samples of the Hettangian sandstone under oxic and anoxic conditions were in the order of magnitude of 1 mg/L, and the solute concentrations of all other elements were one or two orders of magnitude lower (Figs. 2 and 3). In the oxic leaching tests, modest-to-strong positive correlations with temperature ($0.48 < r < 0.88$) and modest-to-strong negative correlations with pH ($-0.6 < r < -0.82$) were observed for all elements except Ca and Cu.

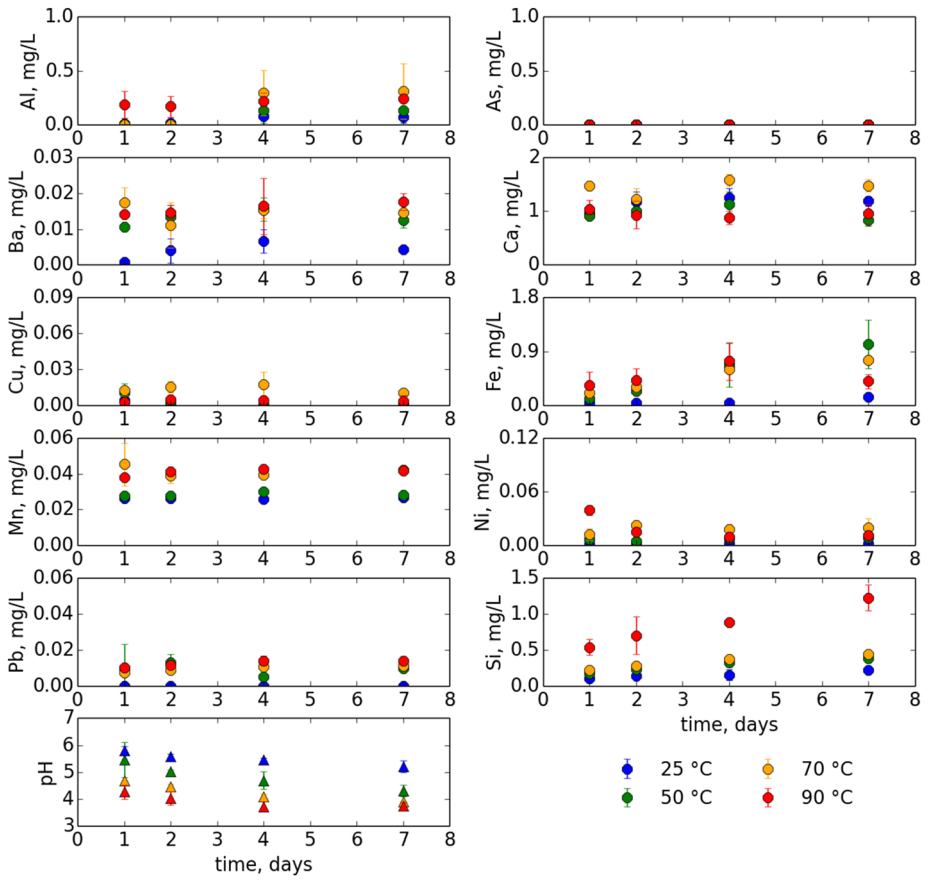

Fig. 2 Extracted elemental concentrations and changes of pH over time observed in the leaching of the Hettangian sandstone under oxic conditions

Under anoxic conditions, in contrast, strong positive correlations with pH were found only for Cu (0.83) and Ni (0.76). Strong positive correlations with temperature were observed for Ba (0.82), Fe (0.74), and Mn (0.95), and a moderate correlation for Si (0.52). Moderate correlations with extraction time were observed for a few elements under oxic conditions (Al, Fe, Si), but not under anoxic conditions. Calcium, Cu, and Pb were only released under oxic conditions (Figs. 2 and 3). While the pH reduction induced moderately or strongly positive correlations between many elements under oxic conditions, only a few strong correlations were calculated under anoxic conditions: Al and Si (0.73), Ba and Mn (0.68), Cu and Ni (0.96), and Fe and Mn (0.86).

During the leaching of the Sinemurian siltstone, the pH decreased over time and with increasing temperature under oxic conditions, and remained nearly constant after 2 days with no temperature effects under anoxic conditions (Figs. 4 and 5). Minimal oxic pH was 3.6 after 7 days at 90 °C, and 5.2 under anoxic conditions. The concentrations of elements released from the Sinemurian siltstone were usually one or two orders of magnitude higher than from the Hettangian sandstone (Figs. 4 and 5). Under oxic conditions, strong negative correlations with pH ($-0.68 < r < -0.99$) were observed for all elements but Cu (-0.28), and strong positive correlations with temperature for Ba (0.82), Ca (0.88), Mn (0.82), Ni (0.68), and Si (0.74). The other elements showed modest

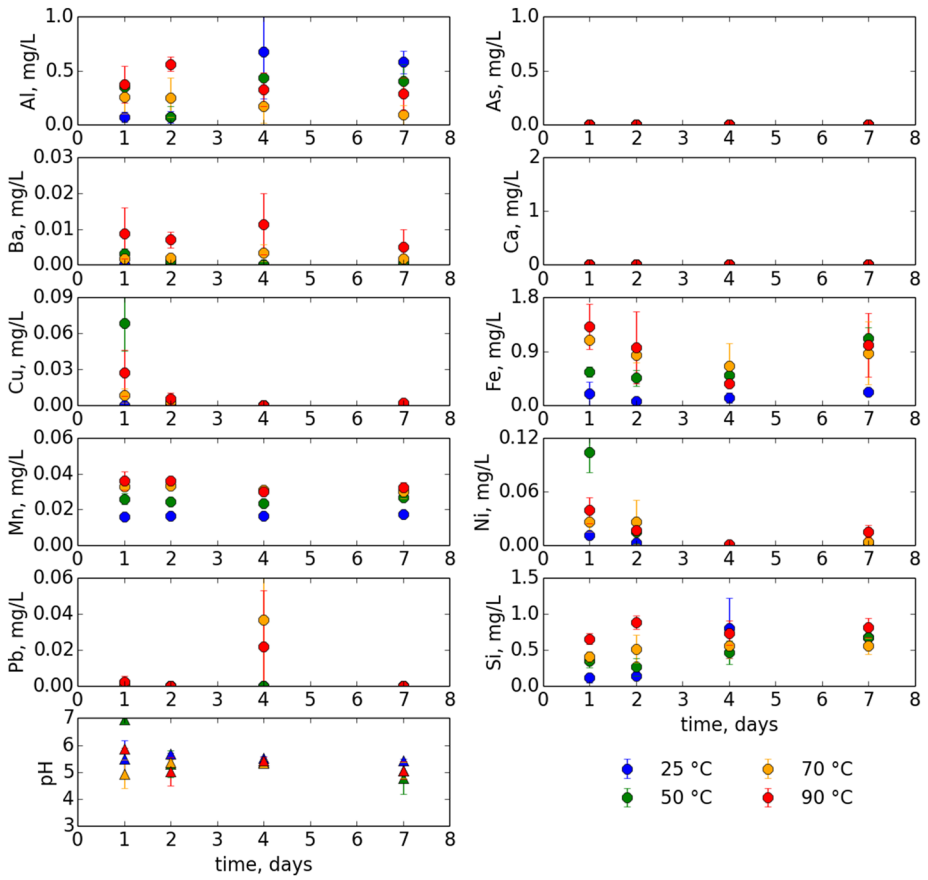

Fig. 3 Extracted elemental concentrations and changes of pH over time observed in the leaching of the Hettangian sandstone under anoxic conditions

temperature correlations, with the exception of Cu, which had none. Similar to the Hettangian sandstone, pH dependencies vanished under anoxic conditions, and only Cu (0.61) and Ni (0.52) showed modest positive correlations. Moderate or strong positive correlations with temperature ($0.41 < r < 0.93$) were observed for all elements except Al (− 0.1), Cu (0.27), and Ni (0.32). The extraction time correlated only moderately with a few elements under oxic conditions (Al, Fe, Ni), while solute concentrations under anoxic conditions did not have significant time trends. Oxic Fe mobilization started only after 2 days at 70 and 90 °C, and almost no Fe was released at lower temperatures (Fig. 4). Aluminum was predominantly released under oxic conditions at 70 and 90 °C, and remained very low at lower temperatures andunder anoxic conditions (Figs. 4 and 5). Similar to the observations made in the leaching of the Hettangian sandstone, solute concentrations of most elements showed moderate or strong positive correlations under oxic conditions. Strong correlations under anoxic conditions were calculated for the releases of Fe, Mn, and Si ($r > 0.85$), and all three elements also had strong positive correlations with Ca ($r > 0.8$). The correlation coefficients between the other elements were mostly moderate.

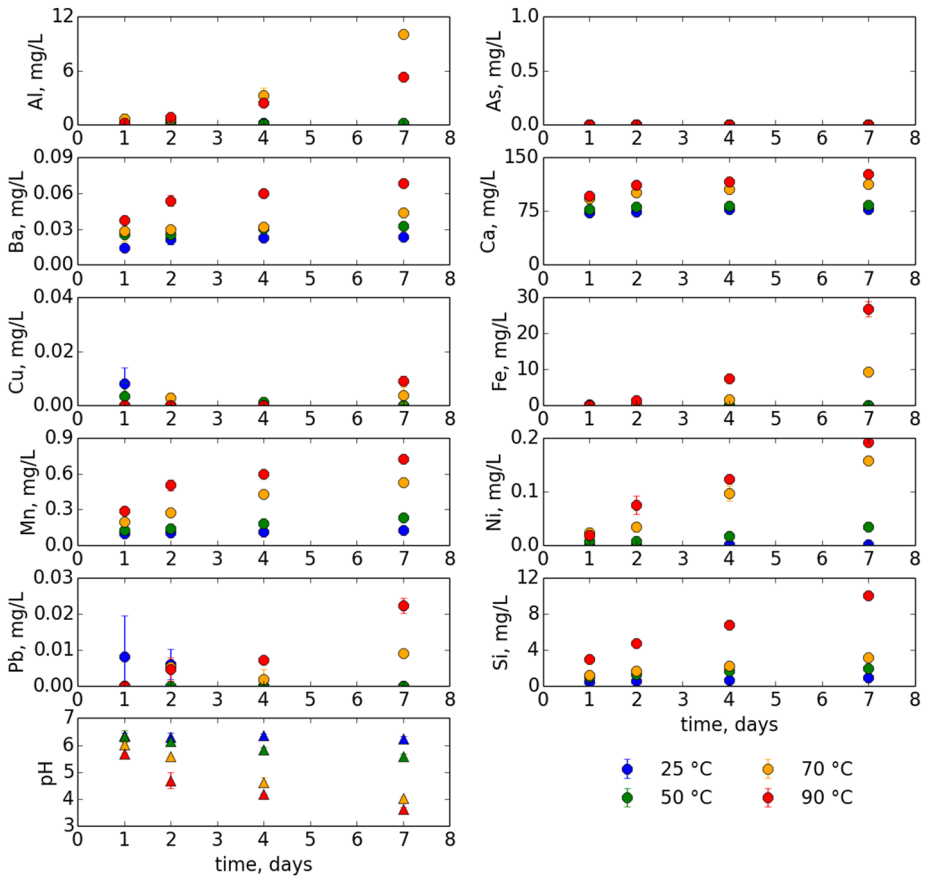

Fig. 4 Extracted elemental concentrations and changes of pH over time observed in the leaching of the Sinemurian siltstone under oxic conditions

Numerical simulation

Simulation results

The NRMSE values (Eq. 2), which describe the difference between simulated and measured ion release, were calculated for Al, Ca, Fe, Mn, and Si. They show that the goodness-of-fit of the simulation tends to be better for oxic than for anoxic conditions, particularly for Fe (Fig. 6). Ca and Mn errors are consistently < 1 for all temperatures. No value was calculated for anoxic Ca mobilization from the Hettangian sandstone, because there was no release under these conditions, and simple temperature-dependent desorption models were not sufficient to explain the observed patterns. However, initial simulations showed that Ca would be released from calcite, if it were present, so it could be deduced that the Hettangian sandstone was calcite-free. NRMSE values for Al release are mostly around 1, although it should be noted that the time trends observed in the leaching of the Sinemurian siltstone could not be reproduced (Figs. 4 and 5). It was found that increasing the reactive surfaces of kaolinite and muscovite within reasonable magnitudes could not explain this issue. The goodness-of-fit of solute Fe and Si concentrations varies with temperature, with the best fits at elevated temperatures (70 and 90 °C). The Fe release could be modeled with a higher precision for oxic than for anoxic conditions, where the observed Fe concentrations were generally strongly underestimated (Fig. 6). In contrast, the solute concentrations and time trends of the oxic leaching tests could

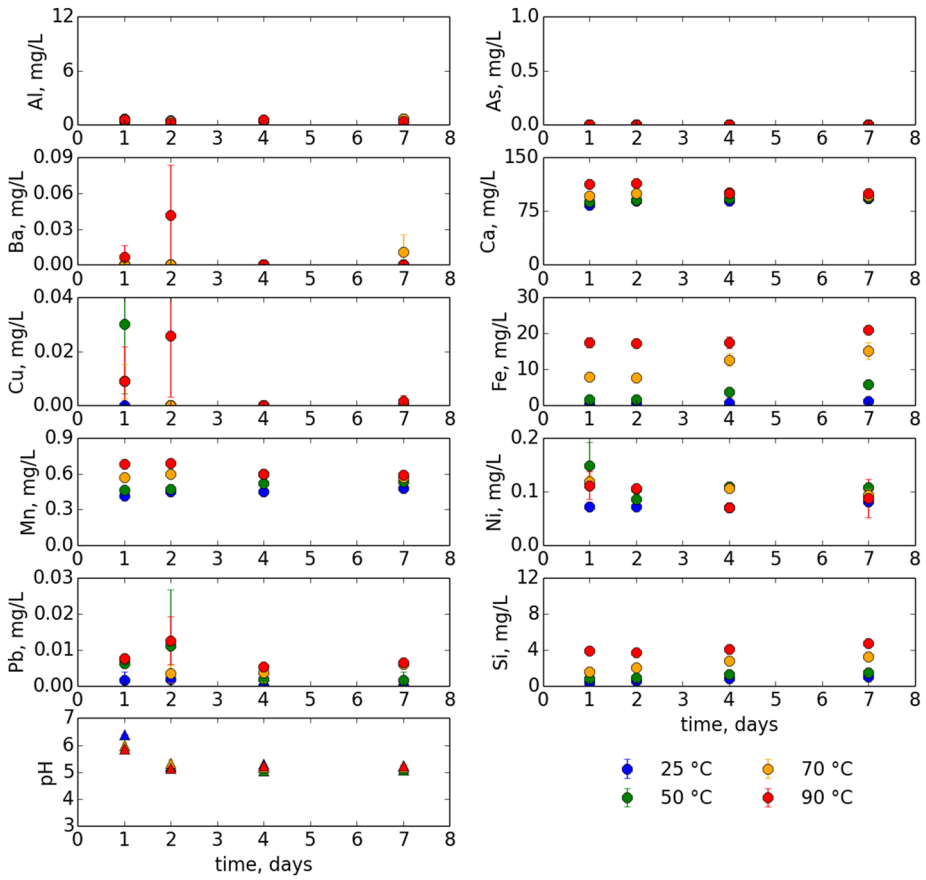

Fig. 5 Extracted elemental concentrations and changes of pH over time observed in the leaching of the Sinemurian siltstone under anoxic conditions

be reproduced well for both rocks by modeling only pyrite dissolution (Fig. 7). Due to precipitation of iron hydroxides and consequent depletion of solute Fe during the 90 °C leaching of the Hettangian sandstone, this data point was excluded from fitting. For the Sinemurian siltstone, reproducing the experimental solute Fe trends required setting a threshold time point at which pyrite dissolution starts, and allow its reactive surface to increase linearly. Time thresholds were set to 50,000 s at 70 °C and 75,000 s at 90 °C. Pyrite dissolution at lower temperatures was set to zero, resulting in large error values, as very small quantities of Fe were released in the leaching tests nevertheless (Fig. 6).

Sensitivity analysis

The calculated values of total-order sensitivities for the release of Fe under oxic conditions show that pyrite dissolution is the main source of solute Fe, while the dissolution of ferrihydrite and changes in the redox potential (pe) are no important factors (Fig. 8). An exception is the 25 °C extraction of the Sinemurian siltstone, where pyrite dissolution was manually disabled to match the experimental results (compare Fig. 7). Under these conditions, pe is the most important input variable.

The calculated sensitivities for solute Si show that its mobilization depends primarily on the dissolution of amorphous silica. At 25 °C, kaolinite and, to a smaller extent,

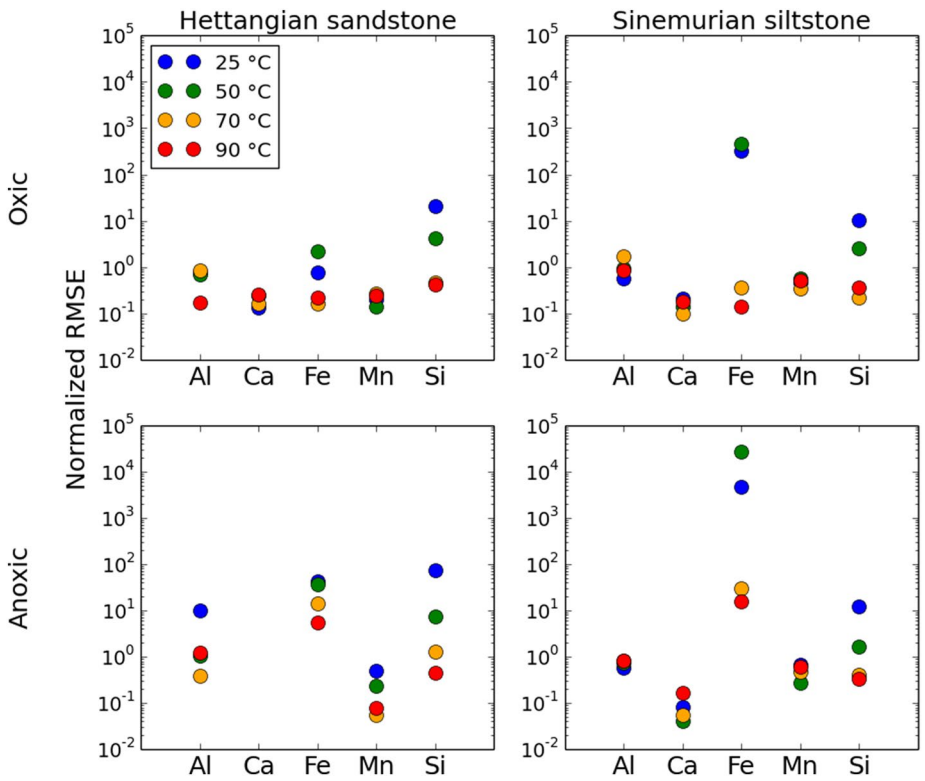

Fig. 6 The calculated normalized root mean square errors (NRMSE) over all time steps for a specific element and temperature showing the goodness-of-fit of the simulations. Anoxic extraction of Ca from the Hettangian sandstone has no NRMSE values, because the extracted amount was zero

muscovite also contribute significantly (Fig. 9). The dissolution of quartz and potassium feldspar within a week is nearly zero. The reduction of pH by pyrite dissolution is insignificant, and direct influences of pe and oxygen availability cannot be observed.

For the mobilization of Al, the sensitivity analysis shows that its main release mechanism at low temperatures is cation exchange, and at elevated temperatures, the dissolution of amorphous aluminum hydroxides (Fig. 10). The sensitivities to the presence of kaolinite and muscovite are minor, and potassium feldspar is insignificant. In contrast, the presence of pyrite is a significant parameter, as it affects dissolution and desorption mechanics of Al-bearing phases. Oxygen and pe have no direct effect.

Discussion

Iron and manganese mobilizations

The release of Mn from both rock types increased with temperature and decreased with pH (Figs. 2, 3, 4, 5). Its mobilization patterns could be modeled precisely under oxic and anoxic conditions, taking ion exchange and the equilibrium dissolution of manganese oxohydroxides into account, although oxohydroxide dissolution was calculated with no value for the standard enthalpy of reaction (Fig. 6). The release of Fe from both rock types under oxic conditions could be explained accurately with the oxidation of pyrite by oxygen and ferric iron (Table 2). Ferrihydrite did not contribute significantly to oxic Fe release, as indicated by the sensitivity analysis (Fig. 8). It was possible to fit the reactive surface of pyrite directly to the solute Fe concentration (Fig. 7), which resulted in plausible

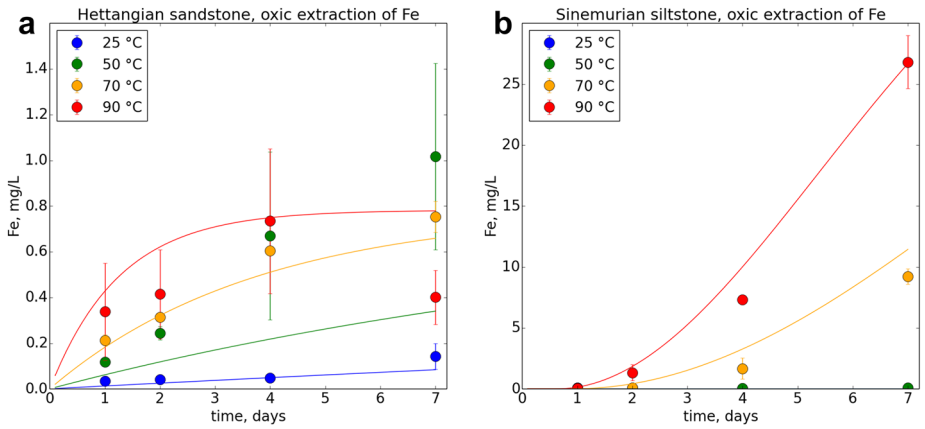

Fig. 7 Simulated (lines) and measured (dots) Fe concentrations released over time during oxic experiments from **a** Hettangian sandstone and **b** Sinemurian siltstone. The normalized root mean square errors for each temperature are shown in Fig. 6

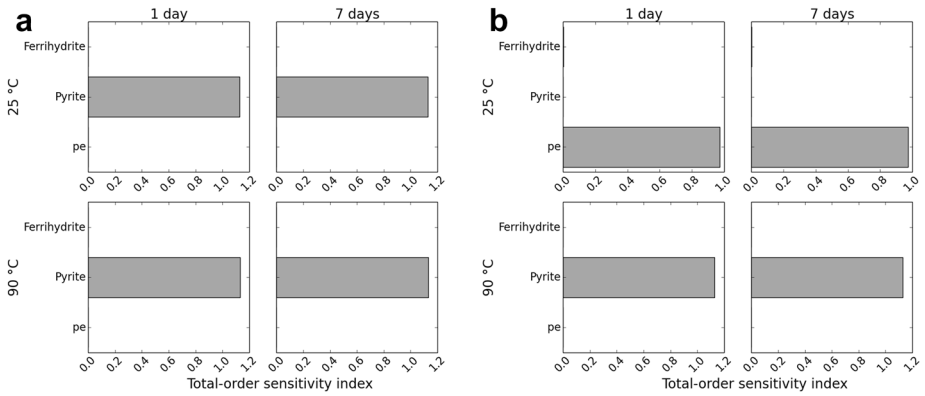

Fig. 8 Calculated total-order sensitivities for oxic Fe release depending on temperature after 1 and 7 days, respectively, from **a** the Hettangian sandstone and **b** the Sinemurian siltstone

reactive surface values of approximately three orders of magnitude lower than the median specific surface values obtained from the RES^{3}T database of the literature values (Brendler et al. 2003). The observed retardation and temperature dependences of oxic Fe release from the Sinemurian siltstone can be explained with amorphous coatings blocking the surfaces of the pyrite crystals, which Müller et al. (2017) identified using SEM–EDX. These coatings had to be removed before pyrite dissolution could start. The release of Fe under anoxic conditions was fast and occurred almost entirely within the first day (Figs. 3 and 5). A comparison of the leached concentrations of up to 1 mg/l (ca. 0.03 mg/g rock) from the Hettangian sandstone (Fig. 3), and 21 mg/l (ca. 0.6 mg/g rock) from the Sinemurian siltstone (Fig. 5) with the total amount of mobile Fe (Fig. 1) shows that only the mobilization of the reducible fraction can explain the leached Fe concentration. This indicates iron (hydr)oxide dissolution. However, it was not possible to simulate the observed iron hydroxide dissolution, using ferrihydrite $Fe(OH)_3$ as a simplified representative phase, with acceptable precision. The released Fe concentrations were underestimated using thermodynamic data from the SIT database (Fig. 6). Thermodynamic data from the LLNL database reproduced the observed anoxic Fe release, but overestimated oxic Fe release in turn. This result suggests that the simplified ferrihydrite phase is insufficient for a precise

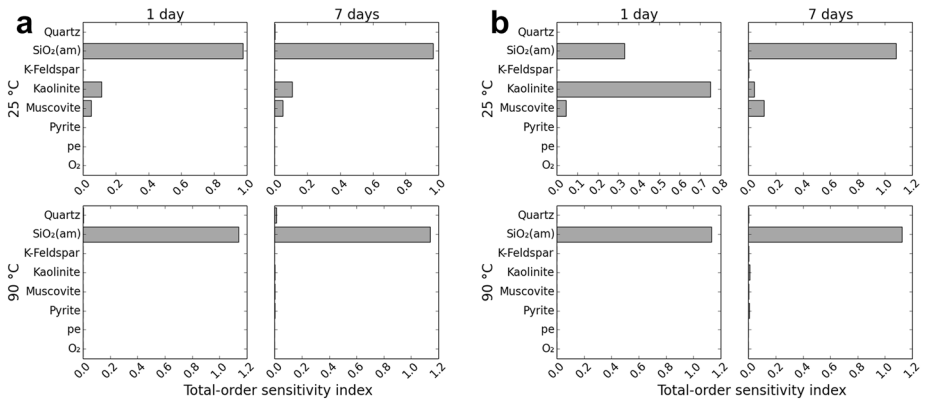

Fig. 9 Calculated total-order sensitivities for Si release depending on temperature after 1 and 7 days, respectively, from **a** the Hettangian sandstone and **b** the Sinemurian siltstone

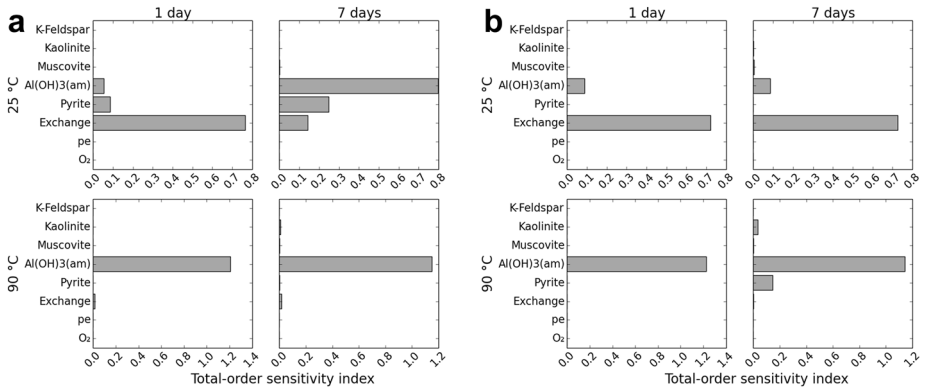

Fig. 10 Calculated total-order sensitivities for Al release depending on temperature after 1 and 7 days, respectively, from **a** the Hettangian sandstone and **b** the Sinemurian siltstone

simulation of the dissolution of iron (hydr)oxides.. Another possible explanation is that the hydroxides of Fe and Mn formed mixed amorphous layers in the investigated rocks (e.g., Mustafa et al. 2002), as suggested by the strong correlation of Fe and Mn release under anoxic conditions. In the Sinemurian siltstone, there is also a strong correlation of Si with Fe and Mnunder anoxic conditions, suggesting that amorphous silica was also incorporated in these layers. It is also possible that microbial reduction of the iron (hydr) oxides occurred (e.g., Kappler et al. 2004), since biofilms were detected in the filters of the ATES well from which the studied rock material was sampled (Huenges 2011). Finally, oven-drying of the rock samples after washing during preparation might have dissolved some pyrite, leaving Fe loosely adsorbed to the grain surfaces of the rocks.

Aluminum and silicium mobilizations

The release of Si during the leaching experiments was initially too fast to be explained with the dissolution of crystalline silicates. In silicate dissolution experiments described in other studies (e.g., Rimstidt and Barnes 1980; Tester et al. 1994), the fast initial release of Si was explained by the highly reactive disturbed surfaces, such as amorphous coatings, edges, kinks, and micrograins, which dissolve quickly before the slower dissolution

of the crystalline matrix starts. The sensitivity analysis performed in the present study confirmed this assumption, as it showed that Si release during the 7 days of the leaching experiments was mainly due to dissolution of amorphous silica (Fig. 9). Its regularly incongruent dissolution might explain the poor goodness-of-fit values calculated for the numerical simulation of Si release (Fig. 6). A second possible effect was suggested by the strong correlation of Si with Mn and Fe in the anoxic extraction of the Sinemurian siltstone, which might be explained by mixed layers of amorphous silica, iron (hydr)oxides and manganese hydroxides, potentially altering the dissolution kinetics of amorphous silica. The mobilization of Al from the Hettangian sandstone could be explained well by combining ion exchange and the equilibrium dissolution of amorphous aluminum hydroxide, while the same explanation overestimated the Al release from the Sinemurian siltstone, and could not reproduce the observed time trends. A possible explanation is that Al hydroxides contained in the siltstone were partially crystalline, while those in the sandstone were entirely amorphous. The quantification of amorphous Al hydroxides applied in this study relies on Al hydroxide dissolution at pH 3.7 (see item 2.3), which will include part of the crystalline Al hydroxides as well (Marion et al. 1975). A second explanation could be the dissolution of highly reactive disturbed surface areas of the Al-bearing minerals kaolinite and muscovite, as already discussed above for Si. The strong correlation between anoxic Si and Al releases from the Hettangian sandstone suggests the dissolution of a solid phase containing both elements (Fig. 3). However, this correlation was not observed for the Sinemurian siltstone, although it could have been masked by other processes such as the dissolution of amorphous silica.

Calcium and barium mobilizations

The release of Ca from the Sinemurian siltstone could be explained well by calcite dissolution and ion exchange (Fig. 6). The strong correlation with Fe, Mn, and Si release under anoxic conditions suggests that Ca was sorbed to the surfaces of the respective hydroxides and amorphous silica. In contrast, Ca release from the Hettangian sandstone differed significantly under oxic and anoxic conditions: oxic release was up to 0.95 mg/L (0.05 mg/g sediment, Fig. 2), indicating that nearly all available mobile Ca was released (Fig. 1), while anoxic release was zero. This was due to sorption reactions, as initial simulations proved that the Hettangian sandstone contains no calcite. The zero release under anoxic conditions suggests that no competitive adsorptions of Na and Ca occurred. Instead, it is likely that Ca was desorbed under oxic conditions because the pH fell below the Ca adsorption edge due to pyrite dissolution (Davis and Kent 1990). Since no Ca was released under anoxic conditions despite the dissolution of Fe and Mn hydroxides, and no correlations between Ca and Fe or Mn were found, it is likely that Ca was sorbed to clay minerals or organic matter rather than to hydroxides. This assumption was not tested by numerical simulations, because the sorbing surface was unknown.

Barium release from both rocks occurred mainly under oxic conditions (Figs. 2, 3, 4, 5). Since the released amounts were higher than the Ba associated with oxidizable phases (Fig. 1), it can be assumed that Ba associated with acid-soluble phases, such as carbonates (Deer et al. 1992) and easily soluble hydroxides, was additionally mobilized by acidification caused by pyrite dissolution.

Mobilizations of other elements

Arsenic was immobile in both investigated rocks (Figs. 2, 3, 4, 5). The sequential extraction identified only small mobile quantities (Hettangian sandstone: 0.01 µg/g, Sinemurian siltstone 2 µg/g, Fig. 1) in oxidizable and reducible phases, and it is likely that released As was below detection limit or re-adsorbed quickly. Copper release was minor and significantly lower than the mobile fraction identified by the sequential extraction (Fig. 1). No strong correlations with mineral-forming elements were found (compare Figs. 2, 3, 4, 5), so that the most likely source is native copper, which was identified in both rocks by Müller et al. (2017). The slightly higher oxic mobilization from both rocks may be explained by the presence of chalcopyrite ($CuFeS_2$), which is a common accessory in pyrite-bearing rocks (Deer et al. 1992). The mobilization patterns of Ni and Pb were comparable for the Sinemurian siltstone. They increased with time and temperature under oxic conditions, and reached equilibrium within one day under anoxic conditions. In the Hettangian sandstone, Pb was associated with oxidizable phases (Fig. 1), and was consequently released only under oxic conditions (Figs. 2 and 3), while Ni showed no distinct release patterns. Both elements are commonly associated with reducible and oxidizable phases, especially with hydroxides, and with sulfides rather than organic matter (Cornell and Schwertmann 1996; Deer et al. 1992; Nissenbaum and Swaine 1976). In the present study, however, no strong correlations with other elements were found, and the exact release mechanisms remain unclear.

Implications for ATES systems

The fluid–rock interactions studied under controlled conditions allow a precise explanation and quantification of the release mechanisms responsible for element mobilization from the studied rocks at up to 90 °C. They help predict how the aquifer will react when specific parameters, such as solute oxygen, change, and if there are risks for aquifer clogging or contaminant mobilization. However, the chemistry of the aquifer during operation will be influenced by several other factors, and elemental mobilization by fluid–rock interactions occurs alongside water mixing and microbial activity, which are the most important contributors to aquifer clogging (e.g., Griebler et al. 2014; Hartog et al. 2013).

The oxic and anoxic cases studied here are boundary cases, and solute oxygen concentration and distribution in the aquifer will be mainly close to the anoxic case ($O_{2(aq)}$ 0–0.25 mg/l, Huenges 2011). Conditions close to the oxic case may either occur in shallow aquifers, or close to the well in deeper aquifers if oxygen leaks into the groundwater during ATES operation. However, nitrogen pressurization, which is common in ATES systems (e.g., Frick et al. 2011; Seibt et al. 2010), should keep solute oxygen concentrations low. Oxygen leaking into the aquifer would furthermore be consumed by oxidizable solute species, e.g., Fe^{2+}, thus reducing solute oxygen available for pyrite dissolution. The issue of groundwater acidification due to pyrite dissolution would be buffered in a natural system, reducing the magnitude of the pH-dependent processes observed in this study. Nitrogen pressurization, oxygen consumption by solute species and groundwater buffering are probably responsible that only minor pH variations between 7.3 and 6.9 were observed in the ATES system aquifer from which the samples of this study were collected (Huenges 2011). However, precipitated iron copper sulfides were found in the filters of the warm well of the system, which can be explained by pyrite dissolution. Severe

precipitation of iron hydroxides after a phase of operation without nitrogen pressurization confirmed this assumption. Pyrite oxidation under anoxic conditions was probably catalyzed by iron-oxidizing microorganisms (*Gallionella* sp.), which were found in groundwater samples (ibid.), and oxidized iron in pH- and solute oxygen ranges in which abiotic pyrite oxidation cannot occur (Eggerichs et al. 2014). Other processes observed in the experiments will be less severe or nonexistent in the ATES system aquifer because of the difference in composition of natural groundwater and synthetic groundwater. For example, measured Ca concentrations in the groundwater during ATES operation ranged between 100 and 150 mg/l (ibid.). It is likely that sorption reactions are at least partially responsible for these shifts, but the exact magnitude is unknown. However, the workflow is capable of reliably excluding risk factors, such as contaminant release. For example, Bonte et al. (2013a) and Javed and Siddique (2016) reported the release of As from rock samples in experiments with elevated temperatures, and showed that the mobilized As had been sorbed to the rock matrix. This could be ruled out for both rocks studied in the present work, since they contained only reducible and oxidizable As, which remained immobile during leaching tests.

Conclusion

The element-release mechanisms of two pyrite-bearing siliciclastic rocks from oxygen-depleted aquifers were investigated with respect to ATES systems, varying temperature, and solute oxygen. A workflow consisting of time-resolved leaching experiments with synthetic groundwater, statistical analyses, and numerical simulations found that

- Oxygen availability controls Fe release from pyrite and iron hydroxides. Only pyrite is dissolved under oxic conditions, and only iron hydroxide is dissolved under anoxic conditions.
- The pH reduction induced by pyrite dissolution governs element mobilization under oxic conditions, e.g., Ca desorption. Under anoxic conditions, element mobilization depends mainly on hydroxide dissolution. Released concentrations are higher under oxic conditions.
- Temperature augments the dissolution of pyrite and hydroxides, and thus all subsequent processes.
- The mobilizations of Al and Si depend strongly on the dissolution of amorphous phases, which dissolve faster at low pH.

The results quantify the sensitivity of an ATES system aquifer to changes in environmental parameters, and can help quantify risks such as iron hydroxide clogging or contaminant release. In general, it was confirmed that the release of most potentially clogging elements and contaminants can be reduced or avoided by preventing oxygen from entering the aquifer, even at elevated temperatures.

Additional file

Additional file 1. Correlation matrices for the extracted element concentrations.

Abbreviations
ATES: aquifer thermal energy storage; NRMSE: normalized root mean square error.

Authors' contributions
DM: experimental work and numerical simulations. SR: consulting and supervision. Both authors read and approved the final manuscript.

Acknowledgements
This work was performed in the framework of the project 'Efficiency and reliability of energy systems in urban districts with seasonal energy storage in aquifers (Aquifer Thermal Energy Storage ATES Berlin)' and was funded by the Federal Ministry for Economic Affairs and Energy (BMWi, 03ESP409A). The authors would like to thank Traugott Scheytt of TU Berlin and Michael Kühn of the University Potsdam for fruitful and interesting discussions. The authors are grateful to Iris Pieper of the geochemical lab at TU Berlin for conducting analyses with ICP-OES. Finally, the authors would like to thank two anonymous reviewers for their valuable comments, which contributed significantly to the quality of this paper.

Competing interests
The authors declare that they have no competing interests.

Availability of data and materials
Data will not be shared. Use in further work planned.

Consent for publication
Not applicable.

Ethics approval and consent to participate
Not applicable.

Funding
This work was supported by the German Federal Ministry for Economic Affairs and Energy (BMWi) under Grant 03ESP409A.

Publisher's Note

Springer Nature remains neutral with regard to jurisdictional claims in published maps and institutional affiliations.

Received: 31 March 2017 Accepted: 20 October 2017
Published online: 11 November 2017

References

Allen RD, Kannberg LD, Raymond JR. Seasonal thermal energy storage. Springfield: Pacific Northwest Laboratory; 1984.
Arning E, Kölling M, Panteleit B, Reichling J, Schulz HD. Einfluss oberflächennaher Wärmegewinnung auf geochemische Prozesse im Grundwasserleiter. Grundwasser. 2006;1(2006):27–39.
Bayer P, Saner D, Bolay S, Rybach L, Blum P. Greenhouse gas emission savings of ground source heat pump systems in Europe: a review. Renew Sustain Energy Rev. 2012;16:1256–67.
Blum P, Campillo G, Münch W, Kölbel T. CO_2 savings of ground source heat pump systems: a regional analysis. Renew Energy. 2010;35:122–7.
Bonte M, van Breukelen BM, Stuyfzand PJ. Temperature-induced impacts on groundwater quality and arsenic mobility in anoxic aquifer sediments used for both drinking water and shallow geothermal energy production. Water Res. 2013a;47:5088–100.
Bonte M, Röling W, Zaura E, van der Wielen PWJJ, Stuyfzand PJ, van Breukelen B. Impacts of shallow geothermal energy production on redox processes and microbial communities. Environ Sci Technol. 2013b;47(24):14476–84.
Brendler V, Vahle A, Arnold T, Bernhard G, Fanghänel T. RES3T-Rossendorf expert system for surface and sorption thermodynamics. J Contam Hydrol. 2003;61:281–91.
Cornell RM, Schwertmann U. The Iron Oxides. Weinheim: VCH Verlagsgesellschaft; 1996.
Davis JA, Kent DB. Surface complexation modeling in aqueous geochemistry. In: White AF, Hochella Jr MF, editors. Mineral-water interface geochemistry. Reviews in mineralogy. Washington DC: Mineralogical Society of America; 1990. p. 177–248.
Deer WA, Howie RA, Zussman J. An introduction to the rock-forming minerals. 2nd ed. Burnt Mill: Longman Scientific & Technical; 1992.
Eggerichs T, Opel O, Otte T, Ruck W. Interdependencies between biotic and abiotic ferrous iron oxidation and influence of pH, oxygen and ferric iron deposits. Geomicrobiol J. 2014;31(6):461–72.
Frick S, Regenspurg S, Kranz S, Milsch H, Saadat A, Francke H, Brandt W, Huenges E. Geochemical and process engineering challenges for geothermal power generation. Chem Ing Tech. 2011;83(12):2093–104.
Fridleifsson IB, Bertani R, Huenges E, Lund JW, Ragnarsson A, Rybach L. The possible role and contribution of geothermal energy to the mitigation of climate change. In: Hohmeyer O, Trittin T editors. In: Proceedings of the IPCC scoping meeting on renewable energy sources. 2009; Lübeck, Germany.vol. 20, no. 25
Griebler C, Kellermann C, Kuntz D, Walker-Hertkorn S, Stumpp C, Hegler F. Auswirkungen thermischer Veränderungen infolge der Nutzung oberflächennaher Geothermie auf die Beschaffenheit des Grundwasser und seiner Lebensgemeinschaften—Empfehlungen für eine umweltverträgliche Nutzung. Dessau-Roßlau: Umweltbundesamt; 2014.

Hähnlein S, Bayer P, Blum P. International legal status of the use of shallow geothermal energy. Renew Sustain Energy Rev. 2010;14:2611–25.
Hartog N, Drijver B, Dinkla I, Bonte M. Field assessment of the impacts of Aquifer Thermal Energy Storage (ATES) systems on chemical and microbial groundwater composition. In: Proceedings of the European Geothermal Conference, Pisa, Italy, 2013.
Herman J, Usher W, Mutel C, Trinidade B, Hadka D, Woodruff M, Rios F, Hyams D. Sensitivity Analysis Library in Python (SALib). 2017. https://github.com/SALib/SALib, https://salib.readthedocs.io. Accessed 30 Mar 2017.
Homma T, Saltelli A. Importance measures in global sensitivity analysis of nonlinear models. Reliab Eng Sys Safe. 1996;52:1–17.
Huenges E (ed) (2011) Thermische Untergrundspeicher in Energiesystemen: Optimierung der Einbindung der Aquiferspeicher in die Wärme- und Kälteversorgung der Parlamentsbauten im Berliner Spreebogen. Helmholtz-Zentrum Potsdam—Deutsches Geoforschungszentrum GFZ, Potsdam.
Javed MB, Siddique T. Thermally released arsenic in porewater from sediments in the cold lake area of Alberta Canada. Environ Sci Technol. 2016;50(5):2191–9.
Jesußek A, Grandel S, Dahmke A. Impacts of subsurface heat storage on aquifer hydrogeochemistry. Environ Earth Sci. 2013;69:1999–2012.
Kappler A, Benz M, Schink B, Brune A. Electron shuttling via humic acids in microbial iron(III) reduction in a freshwater sediment. FEMS Microbiol Ecol. 2004;47:85–92.
Kinniburgh DG, Jackson ML. Concentration and pH dependence of calcium and zinc adsorption by iron hydrous oxide gel. Soil Sci Soc Am J. 1981;46(1):56–61.
Kittrick JA. Soil minerals in the Al_2O_3-SiO_2-H_2O system and a theory of their formation. Clays Clay Miner. 1969;17:157–67.
Kranz S, Bartels J. Simulation and data based identification of parameters affecting seasonal ATES efficiency. In: Proceedings of the 11th international conference on thermal energy storage. Effstock, Stockholm, Sweden, 2009.
Kranz S, Frick S. Efficient cooling energy supply with aquifer thermal energy storage. Appl Energy. 2013;109:321–7.
Lasaga AC. Kinetic theory in the Earth sciences. London: Blackwell; 1998.
Lund JW, Freeston DH, Boyd TD. Direct utilization of geothermal energy 2010 worldwide review. Geothermics. 2011;40:159–80.
Marion GM, Hendricks DM, Dutt GR, Fuller WH. Aluminum and silica solubility in soils. Soil Sci. 1976;121(2):76–85.
McKinney W. Data structures for Statistical Computing in Python. In: Proceedings of the 9th Python in science conference. Austin, TX: SciPy, 2010.
Müller D, Regenspurg S. Geochemical characterization of the lower Jurassic Aquifer in Berlin (Germany) for aquifer thermal energy storage applications. Energy Procedia. 2014;59:285–92.
Müller DR, Friedland G, Regenspurg S. An improved sequential extraction method to determine element mobility in pyrite-bearing siliciclastic rocks. Int J Environ Anal Chem. 2017;97(2):168–88.
Müller M (2013) PhreeqPy Documentation, Release 0.2. http://www.hydrocomputing.com. Accessed 17 Aug 2016.
Mustafa S, Dilara B, Nargis K, Naeem A, Shahida P. Surface properties of the mixed oxides of iron and silica. Colloids Surf A. 2002;205:273–82.
Nissenbaum A, Swaine DJ. Organic matter-metal interactions in recent sediment: the role of humic substances. Geochim Cosmochim Acta. 1976;40:809–16.
Nordstrom DK. Aqueous pyrite oxidation and the consequent formation of secondary iron minerals. In: Kittrick JA, Fanning DS, Hossner LR, editors. Acid sulfate weathering. Madison: Soil Science Society of America; 1982.
Palandri JL, Kharaka YK. A Compilation of Rate Parameters of Water-Mineral Interaction Kinetics for Application to Geochemical Modeling. Menlo Park: US Geological Survey; 2004.
Palmer CD, Blowes DW, Frind EO, Molson JW. Thermal energy storage in an unconfined aquifer 1. Field Injection Experiment. Water Resour Res. 1992;28(10):2845–56.
Parkhurst DL, Appelo CAJ. Description of input and examples for PHREEQC version 3: a computer program for speciation, batch-reaction, one-dimensional transport, and inverse geochemical calculations. 2013. http://pubs.usgs.gov/tm/06/a43. Accessed 17 Jan 2014.
Possemiers M, Huysmans M, Batelaan O. Influence of aquifer thermal energy storage on groundwater quality: a review illustrated by seven case studies. J Hydrol. 2014;2:20–34.
Rimstidt JD, Barnes HL. The kinetics of silica-water reactions. Geochim Cosmochim Acta. 1980;44:1683–99.
Saltelli A. Making best use of model evaluations to compute sensitivity indices. Comput Phys Commun. 2002;145:280–97.
Saltelli A, Annoni P, Azzini I, Campolongo F, Ratto M, Tarantola S. Variance based sensitivity analysis of model output. Design and estimator for the total sensitivity index. Comput Phys Commun. 2010;181:259–70.
Seibt P, Kabus F, Wolfgramm M, Bartels J, Seibt A. Monitoring of hydrogeothermal plants in Germany: an overview. In: Proceedings of the world geothermal congress, Bali, Indonesia, p. 25–29. 2010.
Sobol IM. Global sensitivity indices for nonlinear mathematical models and their Monte Carlo estimates. Math Comput Simulat. 2001;55:271–80.
Sulkowski, A. Speziesanalytische Untersuchungen an Boden- und Sedimentgesteinsproben auf der Grundlage von Extraktions- und Röntgenmethoden. Ph.D. Thesis, Essen (Germany), 2002.
Taylor R. Interpretation of the correlation coefficient: a basic review. J Diagn Med Sonogr. 1990;6(1):35–9.
Tester JW, Worley WG, Robinson BA, Grigsby CO, Feerer JL. Correlating quartz dissolution kinetics in pure water from 25 to 625 °C. Geochim Cosmochim Acta. 1994;58(11):2407–20.
Van der Walt S, Colbert SC, Varoquaux G. The NumPy array: a Structure for efficient numerical computation. Comput Sci Eng. 2011;13:22–30.
Vetter A, Mangelsdorf K, Schettler G, Seibt A, Wolfgramm M, Rauppach K, Vieth-Hillebrand A. Fluid chemistry and impact of different operating modes on microbial community at Neubrandenburg heat storage (Northeast German Basin). Org Geochem. 2012;53:8–15.
Wolfgramm M, Seibt A. Geochemisches Monitoring des geothermalen Tiefenspeichers in Neubrandenburg. In: Proceedings of GtV conference, Karlsruhe, Germany, 2006.

Würdemann H, Westphal W, Lerm S, Kleyböcker A, Teitz S, Kasina M, Miethling-Graff R, Seibt A, Wolfgramm M. Influence of microbial processes on the operational reliability in a geothermal heat store: results of long-term monitoring at a full scale plant and first studies in a bypass system. Energy Procedia. 2014;59:412–7.